Letter

Anapole mechanism of bound states in the continuum in symmetric dielectric metasurfaces

Izzatjon Allayarov [1,2,3,*] Antonio Calà Lesina [1,2,3,†] and Andrey B. Evlyukhin [3,4,‡]

[1]*Hannover Centre for Optical Technologies, Leibniz University Hannover, 30167 Hannover, Germany*
[2]*Institute of Transport and Automation Technology, Leibniz University Hannover, 30823 Garbsen, Germany*
[3]*Cluster of Excellence PhoenixD, Leibniz University Hannover, 30167 Hannover, Germany*
[4]*Institute of Quantum Optics, Leibniz University Hannover, 30167 Hannover, Germany*

(Received 27 March 2024; revised 22 May 2024; accepted 31 May 2024; published 21 June 2024)

We present a general multipole mechanism based on the lattice anapole effect leading to the excitation of high-Q resonances in dielectric metasurfaces with the simplest unit cell (i.e., a unit cell with inversion symmetry containing only one nanostructure) and irradiation conditions (i.e., normal incidence). Using multipole techniques, we show analytically and numerically that these resonances are related to the conversion of bound states in the continuum (BICs) to quasi-BICs by simply changing the metasurface period. It is also shown that BICs and quasi-BICs, in turn, are realized through destructive interference (anapole effect) between multipoles of the same parity. The main advantage of such a conversion BIC to quasi-BIC compared to those proposed earlier is that it does not require distortion of symmetric properties of metasurfaces, special conditions of irradiation, or displacement of elements in composite unit cells. The results obtained give an important insight into the physics of high-Q resonances in meta-optics and can simplify and expand the application of metasurfaces for tunable lasing, nonlinear generation, energy trapping manipulation, and enhanced sensing techniques.

DOI: 10.1103/PhysRevB.109.L241405

Introduction. Recently, many optical effects have been realized and proposed in dielectric metasurfaces [1,2], which serve as the physical basis for technological advances in photonics [3]. One effective way to create metasurface resonances with high-quality factor (Q factor) is related to the eigenmodes of the system with purely real eigenvalues, leading to their infinite Q factor. Such eigenmodes do not have an energetic connection with free space, do not emit electromagnetic energy, and cannot be excited by electromagnetic waves incident from the far field. For this reason, they are called bound states in the continuum (BICs) [4,5]. In metasurface optics, these states are usually divided into two basic groups depending on the conditions of implementation, namely, symmetry protected BICs and accidental BICs [6]. In the first case, a BIC is an eigenmode of a metasurface, the multipole decomposition of which, due to its symmetrical properties, includes only multipole moments that individually do not radiate electromagnetic waves out of the metasurface plane [5,7]. In the second case, accidental BICs can arise in a metasurface only at certain values of its material and geometric parameters. In terms of multipole analysis, these modes include a set of multipole moments that individually can radiate electromagnetic waves from the metasurface, but due to destructive interference between these waves, full radiation is completely absent [5,7].

Since BICs cannot be excited by propagating waves, they do not provide any contribution in the reflection and transmission spectra of metasurfaces (even in numerical modeling). However, their existence and influence can emerge by perturbing the parameters associated with the existence of the BIC. In this case, BICs are transformed into quasi-BICs with a finite Q factor, the value of which is determined by the degree of parameter deviation [8–11]. Currently, several approaches have been demonstrated to convert BIC to quasi-BIC. In the case of symmetrically protected BICs, this can be achieved by breaking the inversion symmetry of the elementary cells of the metasurface [12–15] or by using oblique incidence of external waves [16]. For accidental BICs, their conversion into quasi-BICs can be accomplished by changing the irradiation conditions [16,17] or, as in the case of metasurfaces with a superlattice, by spatial displacement of their sublattices [18–21].

In this paper, we present a general multipole mechanism associated with accidental BICs in symmetrical metasurfaces. Contrary to previously reported approaches, this results in high-Q resonances of quasi-BICs excited under normal incident light in periodic metasurfaces with a single-particle unit cell with inversion symmetry. A clear understanding of this mechanism in metasurfaces of simple geometry can significantly expand the range of their functional applications.

Method and Results. In our approach, we consider two types of symmetrical metasurfaces in the visible part of the spectrum: the first type includes metasurfaces composed of cylindrical particles with the refractive index of diamond or titanium dioxide; the second type refers to metasurfaces made of spherical particles with a refractive index of 3.5 without absorption. The first type includes parameters of real materials and is therefore directly related to possible experimental implementation, the second type of metasurfaces is included for demonstration purposes. However, given that silicon has

*Contact author: izzatjon.allayarov@hot.uni-hannover.de
†Contact author: antonio.calalesina@hot.uni-hannover.de
‡Contact author: evlyukhin@iqo.uni-hannover.de

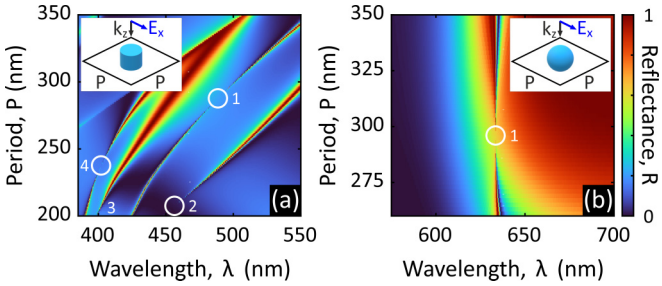

FIG. 1. Reflectance R of infinite metasurfaces as a function of the lattice period P. (a) The metasurface consists of cylinders [diameter $D = 200$ nm, height $H = 300$ nm, refractive index $n_p = 2.45$ (e.g., diamond or titanium dioxide)] placed in a medium with refractive index $n_s = 1.45$. (b) The metasurface consists of spheres (diameter $D = 250$ nm, $n_p = 3.5$) surrounded by a medium with $n_s = 1$. Insets illustrate the corresponding centrosymmetric unit cells. The illumination is a linearly polarized plane wave at normal incidence. The numbered circles show regions with the BICs. Here and all other figures, the values of the wavelength λ are indicated for vacuum.

a refractive index close to 3.5 with negligible absorption in the infrared region, the results on metasurfaces of the second type are also essentially relevant to possible experimental implementation.

Results of numerical simulations of typical optical response of metasurfaces under symmetrical conditions described above are presented in Fig. 1. One can see that the spectral position and width of resonances in reflection can be controlled by selecting the period of a metasurface constructed from symmetrical meta-atoms, such as cylinders [Fig. 1(a)] or spheres [Fig. 1(b)]. Moreover, as will be shown below, the circles with corresponding numbering in the figure indicate the disappearance of the resonances due to accidental BICs.

A. Research approach. Our research analysis of the results in Fig. 1 is based on an important feature of metasurfaces with translational and inversion symmetry: the multipole representation of the interaction (energy exchange) between elementary cells includes multipole moments of only one parity [22]. This leads to the representation of the total optical response of a metasurface at normal light incidence as a superposition of the responses of two noninteracting subsystems, each of which includes either only even multipole moments or only odd ones (see Sec. 1 of the Supplemental Material [33]).

Considering this remark and applying the method of multipole decomposition [2,23–25], the reflection r (and transmission t) coefficient of plane waves by infinite metasurfaces as in Fig. 1, can be expressed in terms of the multipole moments of only one unit cell. For x-polarized incident waves the reflection coefficient can be written as [22,26]

$$r = \frac{\mathrm{i}k_s}{2S_L E_0 \varepsilon_0 \varepsilon_s}\left(p^{\mathrm{eff}} - \frac{1}{v}m^{\mathrm{eff}}\right) = r_{\mathrm{odd}} - r_{\mathrm{even}}, \qquad (1)$$

where k_s and v are the wave number and the speed of light, respectively, in the surrounding medium with relative permittivity ε_s, ε_0 is the vacuum permittivity, S_L is the area of the unit cell, E_0 is the electric field of the external incident wave at the point of multipole moment location in the unit cell. In terms of r_{odd} and r_{even} the transmission coefficient is $t = 1 + r_{\mathrm{odd}} + r_{\mathrm{even}}$, where

$$r_{\mathrm{odd}} = \frac{\mathrm{i}k_s}{2S_L E_0 \varepsilon_0 \varepsilon_s} p^{\mathrm{eff}}, \quad r_{\mathrm{even}} = \frac{\mathrm{i}k_s}{2S_L E_0 \varepsilon_0 \varepsilon_s}\frac{m^{\mathrm{eff}}}{v} \qquad (2)$$

are the odd and even parts of the total reflection coefficient. Here we introduced the effective electric dipole (ED) moment p^{eff}, combining the contribution of the odd multipole moments, and the effective magnetic dipole (MD) moment m^{eff} combining the even multipole contributions, where

$$p^{\mathrm{eff}} = p_x - \frac{\mathrm{i}k_s}{2v}M_{yz} - \frac{k_s^2}{6}O^{(\mathrm{e})}_{xzz} + \ldots \qquad (3)$$

and

$$m^{\mathrm{eff}} = m_y - \frac{\mathrm{i}vk_s}{6}Q_{xz} - \frac{k_s^2}{6}O^{(\mathrm{m})}_{yzz} + \ldots \qquad (4)$$

We can introduce p^{eff} and m^{eff}, since in the above equations all multipole moments [electric **p** and magnetic **m** dipoles, electric $\hat{Q}$ (EQ) and magnetic $\hat{M}$ (MQ) quadrupoles, and electric $\hat{O}^{(\mathrm{e})}$ and magnetic $\hat{O}^{(\mathrm{m})}$ octupoles], regardless of the rank of their tensor, are included in the form of only one component, which generates radiation in the forward and backward directions with the polarization of the incident wave.

As follows from the multipole expansion [see Figs. S1(a)-S1(c) in Sec. 1 of the Supplemental Material [33]], the narrow resonant bands in Fig. 1 are associated with the resonant contribution of either p^{eff} (odd multipoles only) or m^{eff} (only even multipoles) and correspond to either r_{odd} or r_{even}. As a result, the decrease in the width of the resonances and their disappearance in the region indicated by circles in Fig. 1 are determined exclusively by the behavior of either only odd or only even multipoles of the elementary cell of the metasurface. It is important that the contribution of each multipole of the same parity to the corresponding resonant band is of a resonant nature [see Figs. S1(b) and S1(c) in Sec. 1 of the Supplemental Material [33]]. In other words, resonant bands are formed by the overlap of resonances of multipole moments of the same parity. This resonant overlap is associated with the lattice induced energy coupling between multipoles of the same parity in metasurfaces with an inversion-symmetric unit cell [22]: the resonant excitation of some multipoles leads to the resonant excitation of other multipoles of the same parity.

Thus, it becomes clear that due to the corresponding adjustment of the system periodicity, the multipole coupling leads to the spectral points where the resonance width of p^{eff} or m^{eff} goes to zero (the white circles in Fig. 1). These points, as is shown below, correspond to BICs–eigenmodes of the metasurface, which do not radiate into the far-field zone and cannot be excited by external radiation. Multipole analysis of these modes shows that they can include multipoles of only one parity. Moreover, their nonradiating property is realized due to destructive interference between their multipoles, which would individually radiate energy from the system. In the vicinity of points with BICs, these states will transform into quasi-BICs with a finite high-Q factor, as in Fig. 1. To prove the concept of the BICs, we first apply a multipole analytical approach to explain the result in Fig. 1(b) for metasurfaces

composed of spherical particles, and then numerically consider the case of cylindrical particles in Fig. 1(a).

B. Analytical model. Let us consider metasurfaces from Fig. 1(b) made of spherical particles supporting only dipole and quadrupole resonant responses. This fact allows us to apply the coupled dipole-quadrupole approximation developed in [27]. The equations for the dipole (p_x and m_y), and quadrupole (Q_{xz} and M_{yz}) moments of every particle in the metasurface are written as (see Sec. 2 of the Supplemental Material [33])

$$p_x = \alpha_\mathrm{p} E_0 + \frac{\alpha_\mathrm{p}}{\varepsilon_0 \varepsilon_\mathrm{s}} \left(S_\mathrm{pp} p_x + \frac{\mathrm{i}k_\mathrm{s}}{v} S_\mathrm{pM} M_{yz} \right), \tag{5a}$$

$$M_{yz} = \frac{\mathrm{i}k_\mathrm{s}\alpha_\mathrm{M}}{2} H_0 + \frac{\alpha_\mathrm{M}}{2} (-\mathrm{i}v k_\mathrm{s} S_\mathrm{Mp} p_x + S_\mathrm{MM} M_{yz}), \tag{5b}$$

and

$$m_y = \alpha_\mathrm{m} H_0 + \alpha_\mathrm{m} (S_\mathrm{mm} m_y - \mathrm{i}v k_\mathrm{s} S_\mathrm{mQ} Q_{xz}), \tag{6a}$$

$$Q_{xz} = \frac{\mathrm{i}k_\mathrm{s}\alpha_\mathrm{Q}}{2} E_0 + \frac{\alpha_\mathrm{Q}}{2\varepsilon_0 \varepsilon_\mathrm{s}} \left(\frac{\mathrm{i}k_\mathrm{s}}{v} S_\mathrm{Qm} m_y + S_\mathrm{QQ} Q_{xz} \right), \tag{6b}$$

where α_p, α_m, α_Q, α_M are the corresponding dipole and quadrupole polarizabilities of an isolated sphere (for a homogeneous sphere these values are scalar and can be taken from Mie theory); E_0 and H_0 are the external incident electric and magnetic fields, respectively, at the metasurface plane; S_pp, S_mm, S_MM, S_QQ, $S_\mathrm{Mp} = 2S_\mathrm{pM}$, $S_\mathrm{Qm} = 6S_\mathrm{mQ}$ are the ED-ED, MD-MD, MQ-MQ, EQ-EQ, ED-MQ, and MD-EQ lattice sums, respectively, which take into account the interactions between the corresponding multipoles in the metasurface (see Sec. 3 of the Supplemental Material [33]). Note that Eqs. (5) (odd) and Eqs. (6) (even) subsystems are independent of each other. Complete solutions of the above systems and corresponding reflectance are presented in the Sec. 2 of the Supplemental Material [33], where their excellent agreement with the numerical simulation is also demonstrated (see Fig. S2 in Sec. 2 of the Supplemental Material [33]).

Let us now consider in detail the response of only the odd subsystem, since its behavior leads to the narrow resonance in Fig. 1(b). The solution of Eqs. (5) can be presented as

$$p_x = \alpha_\mathrm{p}^\mathrm{eff} E_0 \varepsilon_0 \varepsilon_\mathrm{s}, \quad \text{and} \quad \frac{k_\mathrm{s} M_{yz}}{2\mathrm{i}v} = \alpha_\mathrm{M}^\mathrm{eff} E_0 \varepsilon_0 \varepsilon_\mathrm{s}, \tag{7}$$

where we have introduced the corresponding polarizabilities accounting for the ED-MQ coupling due to S_Mp,

$$\alpha_\mathrm{p}^\mathrm{eff} = \frac{1/\tilde{\alpha}_\mathrm{M} - S_\mathrm{Mp}}{1/[\tilde{\alpha}_\mathrm{M}\tilde{\alpha}_\mathrm{p}] - S_\mathrm{Mp}^2}, \; \alpha_\mathrm{M}^\mathrm{eff} = \frac{1/\tilde{\alpha}_\mathrm{p} - S_\mathrm{Mp}}{1/[\tilde{\alpha}_\mathrm{M}\tilde{\alpha}_\mathrm{p}] - S_\mathrm{Mp}^2}. \tag{8}$$

Here, the $\tilde{\alpha}_\mathrm{p}$ and $\tilde{\alpha}_\mathrm{M}$ polarizabilities take into account only the individual ED-ED and MQ-MQ coupling, respectively,

$$\frac{1}{\tilde{\alpha}_\mathrm{p}} = \frac{\varepsilon_0 \varepsilon_\mathrm{s}}{\alpha_\mathrm{p}} - S_\mathrm{pp}, \quad \frac{1}{\tilde{\alpha}_\mathrm{M}} = \frac{4}{k_\mathrm{s}^2} \left[\frac{1}{\alpha_\mathrm{M}} - \frac{S_\mathrm{MM}}{2} \right], \tag{9}$$

(see also Sec. 2 of the Supplemental Material [33]). Thus, from Eq. (3) and Eq. (7) the effective electric dipole of the odd subsystem is

$$p^\mathrm{eff} = p_x + \frac{k_\mathrm{s} M_{yz}}{2\mathrm{i}v} = (\alpha_\mathrm{p}^\mathrm{eff} + \alpha_\mathrm{M}^\mathrm{eff}) E_0 \varepsilon_0 \varepsilon_s. \tag{10}$$

Introducing the effective odd polarizability

$$\alpha_\mathrm{odd}^\mathrm{eff} = \alpha_\mathrm{p}^\mathrm{eff} + \alpha_\mathrm{M}^\mathrm{eff} = \frac{1/\tilde{\alpha}_\mathrm{p} + 1/\tilde{\alpha}_\mathrm{M} - 2S_\mathrm{Mp}}{1/[\tilde{\alpha}_\mathrm{M}\tilde{\alpha}_\mathrm{p}] - S_\mathrm{Mp}^2}, \tag{11}$$

the reflection coefficient of the odd subsystem r_odd, using Eq. (2) and Eq. (10), can be written as

$$r_\mathrm{odd} = \frac{\mathrm{i}k_\mathrm{s}}{2S_\mathrm{L}} \alpha_\mathrm{odd}^\mathrm{eff}. \tag{12}$$

Thus, the effective odd polarizability $\alpha_\mathrm{odd}^\mathrm{eff}$ determines spectral properties of r_odd. The coefficient r_odd disappears when $p^\mathrm{eff} = 0$ or $\alpha_\mathrm{odd}^\mathrm{eff} = 0$. The latter condition can be reformulated from the numerator of Eq. (11) as

$$\mathrm{Re}(1/\tilde{\alpha}_\mathrm{p} + 1/\tilde{\alpha}_\mathrm{M} - 2S_\mathrm{Mp}) = 0, \tag{13}$$

excluding the case $\mathrm{Re}(1/\tilde{\alpha}_\mathrm{p}) = \mathrm{Re}(1/\tilde{\alpha}_\mathrm{M}) = \mathrm{Re}(S_\mathrm{Mp})$ for which $\alpha_\mathrm{odd}^\mathrm{eff} \neq 0$ (see below). Here we have written the condition in Eq. (13) only for the real part of the numerator, since the same condition for the imaginary part is always satisfied independently on wavelength in the diffractionless ($\lambda > Pn_\mathrm{s}$) region and without ohmic losses in the system, because in this case

$$\mathrm{Im}(1/\tilde{\alpha}_\mathrm{p}) = \mathrm{Im}(1/\tilde{\alpha}_\mathrm{M}) = \mathrm{Im}(S_\mathrm{Mp}) = -k_\mathrm{s}/(2S_\mathrm{L}), \tag{14}$$

for details see Sec. 4 of the Supplemental Material [33].

A spectral dependence of $\alpha_\mathrm{odd}^\mathrm{eff}$ with ($S_\mathrm{Mp} \neq 0$) and without ($S_\mathrm{Mp} = 0$) ED-MQ coupling is shown in Fig. 2(a). It can be seen that the coupling leads to complete suppression of polarizability at the point determined by the condition Eq. (13), creating a narrow suppression band against the background of a wide resonant overlap of $\tilde{\alpha}_\mathrm{p}$ and $\tilde{\alpha}_\mathrm{M}$. The width of the suppression band is estimated by the spectral interval between the zeros of $\alpha_\mathrm{p}^\mathrm{eff}$ and $\alpha_\mathrm{M}^\mathrm{eff}$, which, as follows from Eq. (8), are determined by the equations $1/\tilde{\alpha}_\mathrm{M} - S_\mathrm{Mp} = 0$ and $1/\tilde{\alpha}_\mathrm{p} - S_\mathrm{Mp} = 0$, respectively [see also the inset in Figs. S2(a) in Sec. 2 of the Supplemental Material [33]]. Figure 2(b) shows that between these zero points, $\alpha_\mathrm{p}^\mathrm{eff}$ and $\alpha_\mathrm{M}^\mathrm{eff}$ are out of phase with each other so that at the spectral point defined by Eq. (13), the radiation losses of the odd subsystem were completely suppressed and $\alpha_\mathrm{odd}^\mathrm{eff} = 0$ or $p^\mathrm{eff} = 0$. This behavior is similar to the anapole effect during scattering by a single

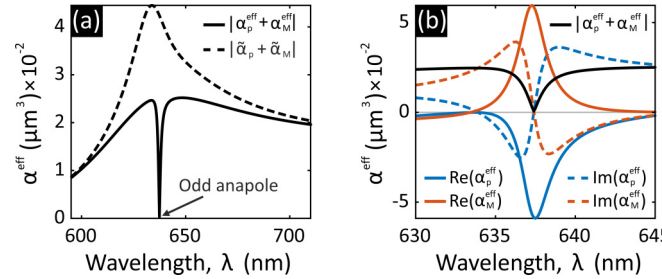

FIG. 2. (a) Absolute values of $\alpha_\mathrm{odd}^\mathrm{eff} = \alpha_\mathrm{p}^\mathrm{eff} + \alpha_\mathrm{M}^\mathrm{eff}$ with (solid line) and without (dashed line) ED-MQ coupling. (b) Polarizabilities $\alpha_\mathrm{p}^\mathrm{eff}$ and $\alpha_\mathrm{M}^\mathrm{eff}$ with ED-MQ coupling. The metasurface parameters are as in Fig. 1(b) and $P = 350$ nm.

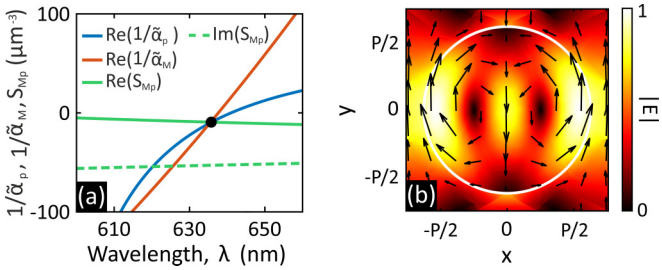

FIG. 3. (a) Numerical visualization of Eq. (16) for the state indicated by the white circle in Fig. 1(b). The imaginary parts overlap. (b) Electric field distribution of the eigenmode at the black point in panel (a). The period of the metasurface is $P = 295$ nm.

particle [28–30]. Indeed, we have suppression of the emission of multipoles of a certain parity from the metasurface due to their destructive interference, while each multipole moment is excited by external waves [4,31]. Thus, we can say that the resonant multipole coupling leads to the lattice anapole effect with respect to the multipoles of a certain parity.

It is important to note that, as followed from Fig. 2(a), the anapole feature appears in the spectral region of overlap of the lattice resonances for the dipole and quadrupole moments, which would exist in the system if coupling were neglected. Therefore, the realization of the anapole mechanism can occur only in those parts of the spectrum where the conditions for lattice resonances of multipoles of different orders are simultaneously satisfied. This is why the anapole mechanism cannot be realized in the pure dipole approximation.

Due to a change in the periodicity of the metasurface, the spectral position of the zeros of $\alpha_{\mathrm{p}}^{\mathrm{eff}}$ and $\alpha_{\mathrm{M}}^{\mathrm{eff}}$ can approach each other, leading to a narrowing of the anapole resonant feature in the reflection spectra. However, when formally the positions of these zeros must coincide, the resonant feature in the reflection will disappear. Let us show that this point corresponds to a BIC.

C. Eigenmode and BIC condition. Eigenmodes of the odd subsystem are the solutions of Eqs. (5), in the absence of the source ($E_0 = H_0 = 0$). Under this condition the system of equations has nontrivial solutions only when its determinant is zero,

$$1 - S_{\mathrm{Mp}}^2 \tilde{\alpha}_{\mathrm{M}} \tilde{\alpha}_{\mathrm{p}} = 0. \tag{15}$$

Its solution providing the condition for the eigenmode existence is (details can be seen in Sec. 5 of the Supplemental Material [33])

$$1/\tilde{\alpha}_{\mathrm{p}} = 1/\tilde{\alpha}_{\mathrm{M}} = S_{\mathrm{Mp}}. \tag{16}$$

Note that Eq. (16) differs from Eq. (13).

Numerical calculation of each term from Eq. (16) for the metasurface with a period of $P = 295$ nm in Fig. 1(b) is shown in Fig. 3(a). One can see that the condition (16) is satisfied for a wavelength $\lambda = 635$ nm, which corresponds to the position of the disappearance of the resonant feature in Fig. 1(b), indicated by a white circle 1. The absence of a resonance at this position in Fig. 1(b) indicates that this eigenmode is not excited by the incident wave. Using a numerical solver for eigenmodes (see Sec. 7 of the Supplemental Material [33]), one can find the distribution of the electric field in a unit cell for this mode: the result is presented in Fig. 3(b).

Since for the eigenmode the electric field is present inside the particles and the nontrivial solution of Eqs. (5) without external fields should satisfy (details in Sec. 5 of the Supplemental Material [33])

$$p^{\mathrm{eff}} = p_x - \frac{\mathrm{i}k_{\mathrm{s}}}{2v} M_{yz} = 0, \tag{17}$$

we have to conclude that $p_x \neq 0$ and $M_{yz} \neq 0$ and the eigenmode is a nonradiating state of the metasurface, i.e., a BIC. Indeed, due to Eq. (17), the effective ED moment p^{eff} of this mode, which includes the multipole moments radiating from the metasurface plane, is zero, ensuring the absence of radiation losses. The physical reason of the suppression of the radiation losses from this mode is the destructive interference between the waves separately emitted by its ED (p_x) and MQ (M_{yz}) moments. This mode is not excited by external waves, and the solution of Eqs. (5) at the condition Eq. (16) is $p^{\mathrm{eff}} = \varepsilon_0 \varepsilon_{\mathrm{s}} E_0 / S_{\mathrm{Mp}} \neq 0$ that differs from Eq. (17).

Note that a similar consideration can be performed for the even subsystem, for which the BIC is a result of the destructive interference between contribution of even multipoles into the far-field radiation [see Figs. S3(a) in Sec. 2 of the Supplemental Material [33], where it is also shown in Figs. S3(e) and Figs. S3(f) that to describe quasi-BIC resonances in the even subsystem of metasurfaces from Fig. 1(b), it is necessary to take into account octupole contributions]. To emphasize the interference mechanism of the appearance of such BICs in symmetric metasurfaces, we will conventionally call them *anapole-odd* BICs or *anapole-even* BICs, depending on the parity of the multipoles involved.

Thus, at the position indicated by the circle in Fig. 1(b), the resonant feature of p^{eff} vanishes because it corresponds to the anapole-odd BIC, which cannot be excited. Away from the pure BIC position, quasi-odd-BICs are realized with the resonant suppression of their p^{eff}. Note that the Fano-type resonant features of the reflectance in Fig. 1(b) at the quasi-odd-BIC are determined by interference between the contributions of resonant p^{eff} and nonresonant m^{eff} [a detail demonstration of this interference is presented in Figs. S3(b)-S3(d) in Sec. 2 of the Supplemental Material [33]]. Furthermore, we note a special behavior of quasi-BIC of the array of spheres. As one can see in Fig. 1(b) (or alternatively in Fig. S2 in Sec. 2 of the Supplemental Material [33]), the spectral position of the quasi-BIC is basically independent of the lattice period and is determined by the MQ resonance of a single sphere with the same diameter and refractive index as in Fig. 1(b).

D. Numerical approach. Now let us show that the established multipole mechanism of the anapole BICs is implemented in a general case of metasurfaces composed of cylindrical particles. Here, as above for the results in Fig. 1, we use ANSYS Lumerical to simulate the optical response of a periodic array of cylindrical particles and COMSOL Multiphysics for eigenfrequency analysis (for details see Sec. 7 of the Supplemental Material [33]). As an example, we will show that the position of the circle 1 in Fig. 1(a) corresponds to the existence of a nonemitting lattice eigenmode with only odd multipoles (anapole-odd BIC). In contrast to the above analytical case, the effective ED moment p^{eff} is approximated as a

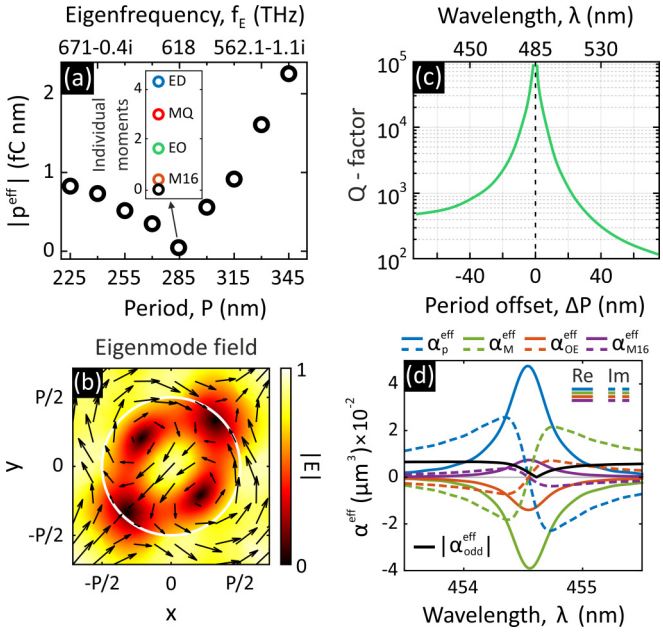

FIG. 4. (a) Dependence of the effective ED moment p^{eff} of the eigenmodes associated with the band indicated by circle 1 in Fig. 1(a), on metasurface period P. The inset shows the absolute values of multipole contributions in p^{eff} of the eigenmode with $p^{\text{eff}} = 0$. (b) Electric field distribution of the nonradiating eigenmode. (c) Quality factor of the resonance band indicated by number 1 in Fig. 1(a) as a function of the period offset $\Delta P = P - P_1$, $P_1 = 285$ nm. (d) Effective polarizabilities of individual odd multipoles from ED up to M16 pole (solid line for the real part, dashed line for the imaginary part; ED: blue lines, MQ: green lines, EO: orange lines, M16: purple lines) and the superposition of the total one $\alpha^{\text{eff}}_{\text{odd}}$ (black line) for the resonant band indicated by number 1 in Fig. 1(a) at $P = 250$ nm.

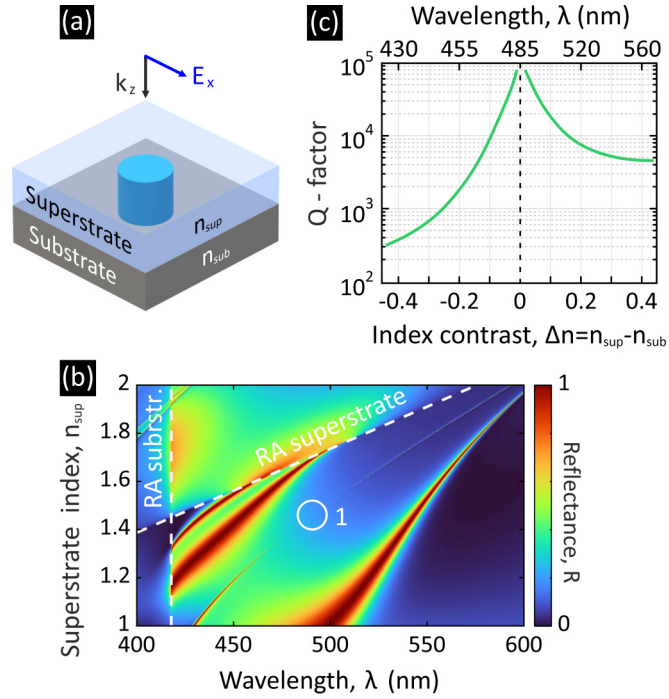

FIG. 5. (a) Sketch of the unit cell of a normally irradiated metasurface with superstrate and substrate. (b) Reflectance of the metasurface with period $P = 285$ nm as a function of the wavelength and the superstrate refractive index. The substrate refractive index is $n_{\text{sub}} = 1.45$. Other parameters of the metasurface as in Fig. 1(a). (c) Dependence of the Q factor of the resonance, indicated by number 1 in panel (b), on the superstrate-to-substrate refractive index contrast $\Delta n = n_{\text{sup}} - n_{\text{sub}}$. The top axis shows the resonance wavelength.

superposition of ED, MQ, EO and magnetic 16th pole (M16) (see Fig. S1 in Sec. 1 of the Supplemental Material [33]). In Fig. 4(a), p^{eff} of that eigenmode for different lattice periods is shown. As one can see, at $P = 285$ nm (the BIC in the circle 1) $p^{\text{eff}} = 0$ and the mode has pure real eigenfrequency $f_{\text{E}} = 618$ THz ($\lambda = 485$ nm), in contrast to the other values of P. Furthermore, as it is shown in the inset, the individual multipole contributions to the effective ED moment p^{eff} are not zero. This proves that this nonradiating mode is an anapole-odd BIC of the system. The electric field distribution of the eigenmode field at the center of the unit cell is presented in Fig. 4(b). Here, we note that due to the symmetry, the eigenstate is degenerate.

The pure BIC has infinite quality factor. However, when deviating from the conditions of the pure BIC, the quality factor of the quasi-BIC depends significantly on the period P of the metasurface. In Fig. 4(c), we see that varying P by ± 10 nm leads to the drop of the Q factor by one order of magnitude. This can have potential applications for optomechanical sensors, for instance, to detect stretching/shrinking of the metasurface environment.

In order to demonstrate in the case of cylindrical particles the anapole mechanism for the formation of resonant (quasi-BIC) bands, we numerically calculated the effective odd polarizability $\alpha^{\text{eff}}_{\text{odd}}$ for the odd resonant quasi-BIC band corresponding to the number 1 of the metasurface with $P = 250$ nm in Fig. 1(a). From the panel Fig. 4(d) it is clear that the complete resonant suppression of $\alpha^{\text{eff}}_{\text{odd}}$ is realized and is a result of a destructive superposition of the corresponding multipole contributions. It is important that the excitation of quasi-BICs is accompanied by an increase in electromagnetic energy in the plane of the metasurface [see Figs. S1(e), S1(f), and S1(h)-S1(j) in Sec. 1 of the Supplemental Material [33]].

E. Influence of a variable superstrate. Finally, let us consider the behavior of anapole-BICs and quasi-BICs in an inhomogeneous environment. As an example, we consider a more practical case with a fixed glass substrate and dynamically variable superstrate. A sketch of the considered metasurface (unit cell) and excitation condition is shown in Fig. 5(a). In Fig. 5(b), the reflectance of the metasurface with period $P = 285$ nm that exhibits odd-anapole BIC, indicated by number 1 in Fig. 1(a), for different superstrate materials is presented. As one sees, a nonradiating pure odd-anapole BIC can be transformed into a radiating quasi-BIC by introducing a refractive index contrast Δn between superstrate and substrate. This is due to the fact that a change in the refractive index of the superstrate leads to a change in the effective wavelength in it and thereby violates the conditions of coupling between multipoles, adding the coupling through reflection from the substrate. As a result, the BIC transforms into quasi-BIC with a spectral shift. The dependence of the

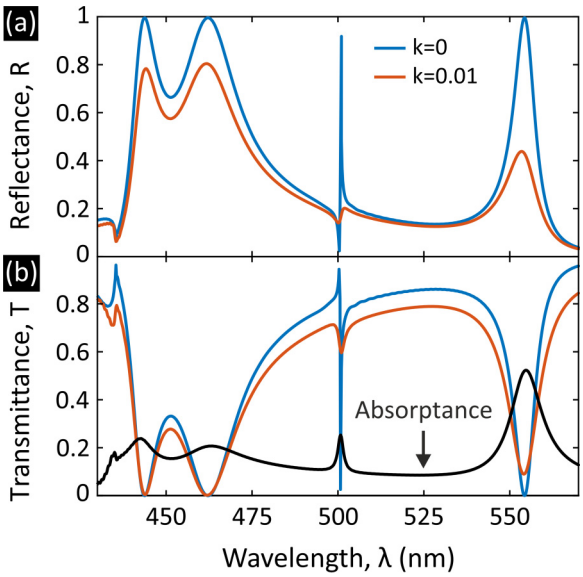

FIG. 6. (a) Reflectance, (b) transmittance and absorptance [black curve in (b)] for the infinite metasurface composed of disks with refractive index of $n_p = 2.45 + ik$ and period $P = 300$ nm. The remaining parameters of the system are as in Fig. 1(a). In the panels, blue and orange curves correspond to $n_p = 2.45$ and $n_p = 2.45 + 0.01i$ ($\varepsilon_p = 6 + 0.05i$), respectively.

quality factor of the odd-anapole BIC on Δn is shown in Fig. 5(c). The Q factor of the odd-anapole BIC is less sensitive to the relative superstrate change $\Delta n/n_{sup}$ than the relative period variation $\Delta P/P_1$. Despite the lower sensitivity, the metasurface can still be used to detect the refractive index change of the surrounding environment, which can be caused by external factors, such as heat or material concentration change.

F. Effect of material absorption and metasurface finite size. In reality, fabricated metasurfaces have nonideal particle shapes, finite sizes, and material impurities that can introduce absorption. These imperfections decrease the Q factor of the metasurface resonance. Since losses are very destructive for the realization of high-Q resonances, below we discuss the influence of the material absorption and radiation losses associated with finite-size structures. For the first case, let us take the system shown in Fig. 1(a) with a certain period, and artificially add a small imaginary part to the disk's refractive index. In Fig. 6, the comparison of the spectrum of the lossless (blue) and lossy (orange) metasurfaces is shown. As one can see, the quasi-BIC of the lossless metasurface (i.e., the narrow resonance at $\lambda = 500$ nm) disappears from the reflectance and transmittance in the presence of the material loss, and interestingly, appears in the absorptance. This means that a quasi-BIC in lossy systems could be identified from the absorption spectrum.

A radiation loss from the edge of a finite-size metasurface can be interpreted as an absorption. Accordingly, in such lossy systems, the realization of high-Q factor resonances, which have long lifetime, can also be problematic. Let us estimate a metasurface size that exhibits a resonance with a certain Q factor. One can define the lifetime of a resonance with Q factor Q and angular frequency ω as $\tau = 2Q/\omega$ (for power dissipation) [32]. Hence, the estimated metasurface size is $d = \tau c/n_s$. Let us consider the narrow resonance (blue curve) at $\lambda = 500$ nm presented in Fig. 6. It has $Q \approx 2000$ and hence $d \approx 225$ μm, which corresponds to an array of 750×750 particles.

Conclusions. We analytically and numerically showed that simple regular dielectric metasurfaces (single particle per unit cell) with inversion symmetry can support high-Q resonant quasi-BICs excited by normally incident light. Quasi-BICs in such systems are associated with the existence of pure accidental BICs, which are eigenmodes with infinite-quality factor and with inclusion of multipole moments of one parity. The developed analytical model for symmetric metasurfaces made it possible to establish a connection between the properties of single particles and the period of the metasurface to determine the conditions for the existence of BICs and quasi-BICs (see Sec. 6 of the Supplemental Material [33]). Since the BICs do not emit waves due to multipole destructive interference, we called them anapole-odd or anapole-even BICs, depending on the involved multipole parity. Changes of the periodicity transforms the pure anapole BICs into quasi-anapole BICs with finite-quality factor. The anapole mechanism responsible for the emergence of BICs and quasi-BICs is purely based on multipole interference and controlled only by lattice period. The configurational and geometric simplicity of symmetrical metasurfaces and the high sensitivity of their quasi-anapole BICs to changes in material and structural parameters make them extremely attractive for the development of multifunctional applications in the fields of linear and nonlinear photonics.

Acknowledgments. We acknowledge the German Research Foundation (DFG, Deutsche Forschungsgemeinschaft) under Germany's Excellence Strategy within the Cluster of Excellence PhoenixD (EXC 2122, Project ID 390833453), and the central computing cluster operated by Leibniz University IT Services (LUIS), which is funded by the DFG (Project No. INST 187/742-1 FUGG).

[1] W. Liu, Z. Li, H. Cheng, and S. Chen, Dielectric resonance-based optical metasurfaces: From fundamentals to applications, iScience **23**, 101868 (2020).

[2] V. E. Babicheva and A. B. Evlyukhin, Multipole lattice effects in high refractive index metasurfaces, J. Appl. Phys. **129**, 040902 (2021).

[3] M. Kang, T. Liu, C. Chan, and M. Xiao, Applications of bound states in the continuum in photonics, Nat. Rev. Phys. **5**, 659 (2023).

[4] K. Koshelev, G. Favraud, A. Bogdanov, Y. Kivshar, and A. Fratalocchi, Nonradiating photonics with resonant dielectric nanostructures, Nanophotonics **8**, 725 (2019).

[5] S. I. Azzam and A. V. Kildishev, Photonic bound states in the continuum: From basics to applications, Adv. Opt. Mater. **9**, 2001469 (2021).

[6] K. Koshelev, A. Bogdanov, and Y. Kivshar, Meta-optics and bound states in the continuum, Sci. Bull. **64**, 836 (2019).

[7] Z. Sadrieva, K. Frizyuk, M. Petrov, Y. Kivshar, and A. Bogdanov, Multipolar origin of bound states in the continuum, Phys. Rev. B **100**, 115303 (2019).

[8] V. A. Fedotov, M. Rose, S. L. Prosvirnin, N. Papasimakis, and N. I. Zheludev, Sharp trapped-mode resonances in planar metamaterials with a broken structural symmetry, Phys. Rev. Lett. **99**, 147401 (2007).

[9] V. R. Tuz, V. V. Khardikov, A. S. Kupriianov, K. L. Domina, S. Xu, H. Wang, and H.-B. Sun, High-quality trapped modes in all-dielectric metamaterials, Opt. Express **26**, 2905 (2018).

[10] K. Koshelev, S. Lepeshov, M. Liu, A. Bogdanov, and Y. Kivshar, Asymmetric metasurfaces with high-Q resonances governed by bound states in the continuum, Phys. Rev. Lett. **121**, 193903 (2018).

[11] A. Barreda, C. Zou, A. Sinelnik, E. Menshikov, I. Sinev, T. Pertsch, and I. Staude, Tuning and switching effects of quasi-BIC states combining phase change materials with all-dielectric metasurfaces, Opt. Mater. Express **12**, 3132 (2022).

[12] L. Xu, K. Zangeneh Kamali, L. Huang, M. Rahmani, A. Smirnov, R. Camacho-Morales, Y. Ma, G. Zhang, M. Woolley, D. Neshev *et al.*, Dynamic nonlinear image tuning through magnetic dipole quasi-BIC ultrathin resonators, Adv. Sci. **6**, 1802119 (2019).

[13] A. B. Evlyukhin, V. R. Tuz, V. S. Volkov, and B. N. Chichkov, Bianisotropy for light trapping in all-dielectric metasurfaces, Phys. Rev. B **101**, 205415 (2020).

[14] N. Bonod and Y. Kivshar, All-dielectric Mie-resonant metaphotonics, C. R. Phys. **21**, 425 (2020).

[15] A. B. Evlyukhin, M. A. Poleva, A. V. Prokhorov, K. V. Baryshnikova, A. E. Miroshnichenko, and B. N. Chichkov, Polarization switching between electric and magnetic quasi-trapped modes in bianisotropic all-dielectric metasurfaces, Laser Photonics Rev. **15**, 2100206 (2021).

[16] D. R. Abujetas, J. Olmos-Trigo, J. J. Sáenz, and J. A. Sánchez-Gil, Coupled electric and magnetic dipole formulation for planar arrays of particles: Resonances and bound states in the continuum for all-dielectric metasurfaces, Phys. Rev. B **102**, 125411 (2020).

[17] D. R. Abujetas, J. Olmos-Trigo, and J. A. Sánchez-Gil, Tailoring accidental double bound states in the continuum in all-dielectric metasurfaces, Adv. Opt. Mater. **10**, 2200301 (2022).

[18] R.-L. Chern, H.-C. Yang, and J.-C. Chang, Bound states in the continuum in asymmetric dual-patch metasurfaces, Opt. Express **31**, 16570 (2023).

[19] T. Shi, Z.-L. Deng, Q.-A. Tu, Y. Cao, and X. Li, Displacement-mediated bound states in the continuum in all-dielectric superlattice metasurfaces, PhotoniX **2**, 7 (2021).

[20] L. M. Berger, M. Barkey, S. A. Maier, and A. Tittl, Metallic and all-dielectric metasurfaces sustaining displacement-mediated bound states in the continuum, Adv. Opt. Mater. **12**, 2301269 (2024).

[21] S. You, M. Zhou, L. Xu, D. Chen, M. Fan, J. Huang, W. Ma, S. Luo, M. Rahmani, C. Zhou *et al.*, Quasi-bound states in the continuum with a stable resonance wavelength in dimer dielectric metasurfaces, Nanophotonics **12**, 2051 (2023).

[22] I. Allayarov, A. B. Evlyukhin, and A. Calà Lesina, Multiresonant all-dielectric metasurfaces based on high-order multipole coupling in the visible, Opt. Express **32**, 5641 (2024).

[23] F. J. García de Abajo, *Colloquium*: Light scattering by particle and hole arrays, Rev. Mod. Phys. **79**, 1267 (2007).

[24] R. Alaee, C. Rockstuhl, and I. Fernandez-Corbaton, Exact multipolar decompositions with applications in nanophotonics, Adv. Opt. Mater. **7**, 1800783 (2019).

[25] P. D. Terekhov, V. E. Babicheva, K. V. Baryshnikova, A. S. Shalin, A. Karabchevsky, and A. B. Evlyukhin, Multipole analysis of dielectric metasurfaces composed of nonspherical nanoparticles and lattice invisibility effect, Phys. Rev. B **99**, 045424 (2019).

[26] R. Dezert, P. Richetti, and A. Baron, Complete multipolar description of reflection and transmission across a metasurface for perfect absorption of light, Opt. Express **27**, 26317 (2019).

[27] V. E. Babicheva and A. B. Evlyukhin, Analytical model of resonant electromagnetic dipole-quadrupole coupling in nanoparticle arrays, Phys. Rev. B **99**, 195444 (2019).

[28] V. Savinov, N. Papasimakis, D. Tsai, and N. Zheludev, Optical anapoles, Commun. Phys. **2**, 69 (2019).

[29] E. A. Gurvitz, K. S. Ladutenko, P. A. Dergachev, A. B. Evlyukhin, A. E. Miroshnichenko, and A. S. Shalin, The high-order toroidal moments and anapole states in all-dielectric photonics, Laser Photonics Rev. **13**, 1800266 (2019).

[30] R. Colom, R. McPhedran, B. Stout, and N. Bonod, Modal analysis of anapoles, internal fields, and Fano resonances in dielectric particles, J. Opt. Soc. Am. B **36**, 2052 (2019).

[31] J. S. T. Gongora, G. Favraud, and A. Fratalocchi, Fundamental and high-order anapoles in all-dielectric metamaterials via Fano–Feshbach modes competition, Nanotechnology **28**, 104001 (2017).

[32] B. E. Saleh and M. C. Teich, *Fundamentals of Photonics* (John Wiley & Sons, Hoboken, NJ, 2019).

[33] See Supplemental Material at http://link.aps.org/supplemental/10.1103/PhysRevB.109.L241405 for effective odd and even polarizabilities (Sec. S1); explicit form of the lattice sums (Sec. S2); details of the derivation of the coupled dipole-quadrupole equations (Sec. S3); relation between imaginary parts of the effective polarizabilities and dipole-quadrupole lattice sum (Sec. S4); derivation of the eigenmode condition and eigensolutions (Sec. S5), including for even subsystem; useful expressions to predict quasi-BICs position (Sec. S7); details of ANSYS Lumerical and COMSOL Multiphysics simulations.